HAL
open science

Electrosynthesis and X-ray Crystallographic Structure of Zn II meso -Triaryltriphenylphosphonium Porphyrin and Structural Comparison with Mg II meso -Triphenylphosphonium Porphine

Abdou Dimé, Hélène Cattey, Dominique Lucas, Charles H. Devillers

To cite this version:

Abdou Dimé, Hélène Cattey, Dominique Lucas, Charles H. Devillers. Electrosynthesis and X-ray Crystallographic Structure of Zn II meso -Triaryltriphenylphosphonium Porphyrin and Structural Comparison with Mg II meso -Triphenylphosphonium Porphine. European Journal of Inorganic Chemistry, 2018, 2018 (44), pp.4834-4841. 10.1002/ejic.201801142 . hal-02071020

HAL Id: hal-02071020

https://hal.science/hal-02071020v1

Submitted on 8 Nov 2021

HAL is a multi-disciplinary open access archive for the deposit and dissemination of scientific research documents, whether they are published or not. The documents may come from teaching and research institutions in France or abroad, or from public or private research centers.

L'archive ouverte pluridisciplinaire **HAL**, est destinée au dépôt et à la diffusion de documents scientifiques de niveau recherche, publiés ou non, émanant des établissements d'enseignement et de recherche français ou étrangers, des laboratoires publics ou privés.

Electrosynthesis and X-ray crystallographic structure of Zn(II) *meso*-triaryltriphenylphosphonium porphyrin and structural comparison with Mg(II) *meso*-triphenylphosphonium porphine

Abdou K. D. Dimé,[a,b] Hélène Cattey,[a] Dominique Lucas[a] and Charles H. Devillers*[a]

Abstract: The electrochemical oxidation of Zn(II) *5,15*-bis(*p*-tolyl)-*10*-phenylporphyrin (**1-Zn**) in the presence of triphenylphosphine (PPh_3) leads to the *meso*-substituted triphenylphosphonium porphyrin, coordinated by one $P(O)Ph_3$ molecule (**1-Zn-PPh$_3^+$,PF$_6^-$·P(O)Ph$_3$**) in good yield (84%). This cationic porphyrin was characterized by NMR, MALDI-TOF mass spectrometry, UV-Vis. absorption spectroscopy and X-ray diffraction analyses. The molecular structure of this compound was compared with already published *meso*- and β-triphenylphosphonium porphyrins but also with an unpublished X-ray crystallographic structure of Mg(II) 5-triphenylphosphoniumporphine (**MgP-PPh$_3^+$,PF$_6^-$**) previously obtained by electrosynthesis.

Introduction

Porphyrins have been the subject of intense researches in numerous fields due to their essential role in natural processes such as photosynthesis and oxygen transport in blood.[1] These macrocycles find applications in material science, (electro)catalysis and energy converting devices.[2] Considerable efforts have been devoted to the functionalization of the porphyrin periphery in β and/or *meso* position(s) with halides, heteroatoms, metals or with other C-C coupled (hetero)aromatic fragments, in order to provide novel functionalities. Among the different heteroatoms, phosphorus-based porphyrins are relatively scarce in the literature, as very recently reviewed by Matano.[3] Four phosphorus-based functional groups exist: phosphino R_2P-), phosphonio (R_3P^+-), phosphoryl ($R_2P(E)$- with R = aryl, alkoxy, E = O, S, Se) and phosphono ($(HO)_2P(O)$-). The introduction of the phosphorus atom is mainly performed using Pd(II or 0)[4] or Cu(I)[4h, 5] coupling with "activated" (-OTf, -I, -Br) β and/or *meso* substituted porphyrins. Recently, Osuka and co-workers synthesized a *meso*-substituted diphenylphosphino-porphyrin nickel(II) complex *via* an aromatic nucleophilic substitution of *meso*-chloroporphyrin with $LiPPh_2$.[4j] Among these phosphorus-based porphyrins, the sole synthetic pathway to phosphonio-porphyrins lies on the chemical/electrochemical oxidation of the porphyrin macrocycle in the presence of a tertiary phosphine. These porphyrins may find medical applications as tumor imaging agents and mitochondrial targeting molecules as aryl-phosphonium derivatives have both lipophilic and cationic character. This feature allows for their facile transport through plasma membranes or cell walls to accumulate in the cytoplasm or cell mitochondria.[6] In a pioneer work, Smith and co-workers reported that triphenylphosphine (PPh_3) can react as a nucleophile in *meso* position with the cation radical of the Zn(II) octaethylporphyrin complex (ZnOEP) preliminary generated by oxidation with magic blue (tris(4-bromophenyl)ammonium hexachloroantimonate)[7] while Shine and co-workers[8] described the β-position reactivity of the zinc(II) tetraphenylporphyrin (ZnTPP) cation radical (chemically generated by oxidation with $I_2/AgClO_4$) with PPh_3. Later, Latos-Grażyński and co-workers reported the chemical β-functionalization of preformed $(TPP)Fe^{III}(ClO_4)_2$ with PPh_3 that afforded the $[(\beta\text{-}PPh_3^+\text{-}TPP)Fe^{III}]_2O(ClO_4)_2$ dimer.[9] In all cases, *meso*- and β-phosphonium-based porphyrins were generated in modest yields (≤ 37.7%). A significant progress in the yield of phosphonium-based porphyrins was achieved by Giraudeau *et al.* when they continuously generated the porphyrin π-cation radical in presence of PPh_3 by controlled potential electrolysis. In these conditions, β-PPh_3^+-ZnTPP,ClO_4^- was generated in 50% yield.[10] The same group further exploited the electrogenerated ZnTPP cation radical reactivity with a bisphosphine base (bis(diphenylphosphino)acetylene) providing the mono phosphonium porphyrin and/or the bisphosphonium porphyrin dimer in fair to good yield, depending on the amount of the nucleophile.[11] This work was extended to other bis- and trisphosphine nucleophiles leading to bis(β-phosphonium)-ZnTPP dimers and tris-(β-phosphonium)-ZnTPP trimers in good yield (60-93%).[12] As part of our on-going interest focused on the redox reactivity of porphine, the fully unsubstituted porphyrin,[13] we functionalized magnesium(II) porphine (**MgP**) with PPh_3 by controlled potential electrolysis and obtained the *meso*-triphenylphosphonium porphyrin (**MgP-PPh$_3^+$,PF$_6^-$**) in good yield (78%). This latter was the first X-ray crystallographic structure example of *meso*-phosphonium porphyrin.[14] In this particular case, a large excess of phosphine was necessary to prevent the competitive **MgP** oxidative polymerization from occurring.[15] In order to decrease the propensity to polymerize and to favor the anodic nucleophilic substitution reaction, more recently we synthesized the *5,15*-bis(*p*-tolyl)-*10*-phenylporphyrin (**1-H$_2$**) which has only one available free *meso* position. The electrochemical oxidation in the presence of PPh_3 of the corresponding Ni(II)

[a] Dr. A. K. D. Dimé, Dr. H. Cattey, Pr. Dr. D. Lucas, Dr. C. H. Devillers
Institut de Chimie Moléculaire de l'Université de Bourgogne UMR CNRS 6302, Université Bourgogne Franche-Comté, 9 Avenue Alain Savary, 21078 Dijon cedex, France
E-mail: charles.devillers@u-bourgogne.fr, http://icmub.com
[b] Dr. A. K. D. Dimé,
Département de Chimie, UFR SATIC, Université Alioune Diop de Bambey, Senegal

Supporting information for this article is given via a link at the end of the document.

WILEY-VCH

complex (**1-Ni**) led to the *meso*-PPh_3^+-porphyrin (**1-Ni-PPh$_3^+$,PF$_6^-$**) in 72% yield.[16]

In this manuscript will be presented the extension of this work to the Zn(II) complex, **1-Zn**, providing the novel *meso*-PPh_3^+-porphyrin (**1-Zn-PPh$_3^+$,PF$_6^-$·P(O)Ph$_3$**) in good yield. The electrolysis is monitored by cyclic voltammetry and UV-Vis. absorption spectroelectrochemistry. X-ray crystallographic analyses reveal that the zinc cation is O-coordinated by one triphenylphosphine oxide molecule. Comparison of this X-ray crystallographic structure with previously published (**1-Ni-PPh$_3^+$,PF$_6^-$**[16] and **MgP-PPh$_3^+$,PF$_6^-$**[14]) and unpublished (**MgP-PPh$_3^+$,PF$_6^-$**, other crystallization conditions) *meso*-triphenylphosphonium porphyrins molecular structures will be presented.

Results and Discussion

Electrochemical investigations

Cyclic voltammetry

The cyclic voltammogram (CV) of **1-Zn** in CH_2Cl_2/CH_3CN mixture (4/1 v/v) 0.1 M $TEAPF_6$ (solid blue line, Fig. 1) exhibits one monoelectronic reversible oxidation leading to the cation-radical at $E_{1/2}$ (O1/R1) = 0.86 V (ΔE_p = 75 mV) and one reversible monoelectronic reduction leading to the radical anion species $E_{1/2}$ (O2/R2) = −1.40 V (ΔE_p = 90 mV, all potentials given in this manuscript will be given *vs*. the saturated calomel electrode (SCE); in these experimental conditions, ferrocene is oxidized at 0.40 V). [17]

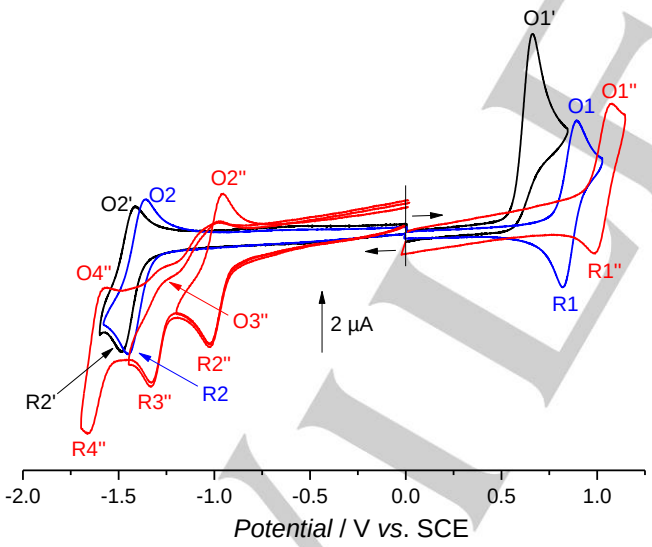

Figure 1. Cyclic voltammograms of **1-Zn** with (solid black line) or without (solid blue line) 20 eq. of PPh_3 and **1-Zn-PPh$_3^+$,PF$_6^-$** with 20 eq. PPh_3 (solid red line) in CH_2Cl_2/CH_3CN (4/1 v/v) 0.1 M $TEAPF_6$. Concentration: 5×10^{-4} M; WE: Pt Ø = 2 mm, ν = 100 mV s^{-1}.

The second reduction stage of the porphyrin ring is not observed since it falls beyond the solvent reduction. Indeed, when 20 eq. of PPh_3 are added to the solution, the first oxidation process (E_{pa}(O1') = 0.66 V) becomes irreversible with a two-fold more intense peak current than the one observed for the reversible reduction ($E_{1/2}$(O2'/R2') = −1.45 V, ΔE_p = 70 mV). Moreover, peak O1' is shifted towards less positive potential (E_{pa}(O1)-E_{pa}(O1') = −0.23 V). This behavior arises from two phenomena: 1) the initially generated cation radical **1-Zn$^{\cdot+}$** undergoes a fast chemical reaction with PPh_3 followed by a subsequent one electron uptake (ECE-type mechanism)[14, 18]; 2) the coordination of PPh_3 to the Zn(II) cation which increases the porphyrin electronic density and makes it easier to oxidize and more difficult to reduce, as it can be seen on the first reduction peak (compare peaks R2 and R2'). The CV of a pure sample of **1-Zn-PPh$_3^+$,PF$_6^-$·P(O)Ph$_3$** in the same experimental conditions (*i.e.* with 20 eq. PPh_3) exhibits a monoelectronic reversible oxidation leading to the cation-radical ($E_{1/2}$(O1''/R1'') = 1.03 V, ΔE_p = 90 mV). In the negative potential direction, the first monoelectronic reversible peak ($E_{1/2}$(O2''/R2'') = −0.99 V, ΔE_p = 70 mV) may be attributed to the first reduction of the porphyrin ring since the potential difference between the first oxidation and reduction (HOMO–LUMO gap, $\Delta E_{1/2}$ = 2.02 V) fall within the empirical value of 2.15 ± 0.15 V previously reported for octaethylporphyrin complexes.[19] The CV exhibits two others reductions at E_{pc}(R3'') = −1.33 V and E_{pc}(R4'') = −1.66 V which plausibly correspond to the reduction of the phosphonium and the porphyrin ring moieties, respectively.

Electrosynthesis

Electrolyses were carried out under argon, at room temperature, in a CH_2Cl_2/CH_3CN mixture (4/1 v/v) containing 0.1 M of $TEAPF_6$, **1-Zn**, 20 eq. of PPh_3 and 10 eq. of 2,6-lutidine. This non-nucleophilic base is added to trap the protons released in the course of the reaction; otherwise demetalation of Zn(II) porphyrin could occur. Starting with 20.0 mg of **1-Zn** the potential was set at E_{app} = 0.70 V. The current progressively decreased and finally reached the residual current value when 2.4 F per mol of **1-Zn** were transferred. After removal of the supporting electrolyte, purification of the crude product on silica gel and crystallization from toluene, the *meso*-triphenylphosphonium porphyrin **1-Zn-PPh$_3^+$,PF$_6^-$·P(O)Ph$_3$** was isolated in 84% yield (Scheme 1).

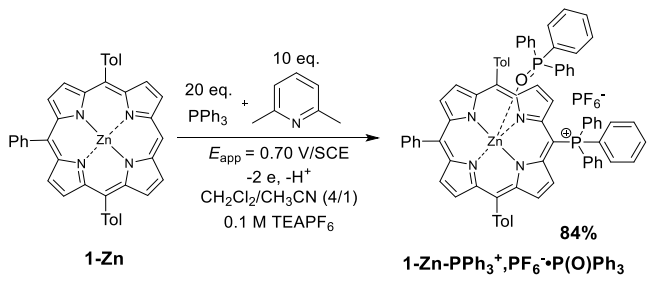

Scheme 1. Electrochemical synthesis of **1-Zn-PPh$_3^+$,PF$_6^-$·P(O)Ph$_3$**.

We tried to diminish the amount of phosphine nucleophile up to two equivalents. Though the reaction was still efficient, the competing oxidative *meso-meso* dimerization process was observed on the UV-Vis. absorption spectrum, as attested by the

characteristic Soret band of the *meso-meso*-linked dimer **2-Zn** at 459 nm.[17a] The presence of coordinated phosphine oxide was unexpected. However, the purity of the initial PPh_3 was 99% and contained less than 1% triphenylphosphine oxide $P(O)Ph_3$. Thus, in our conditions, less than 0.2 eq. of $P(O)Ph_3$ is initially present in the solution to be electrolyzed. The missing $P(O)Ph_3$ amount may be formed during the electrolysis (oxidation of PPh_3 in presence of trace amount of water leads to $P(O)Ph_3$[20]) and/or might be produced during the work-up (extraction of the supporting electrolyte with several aqueous washings under an air atmosphere).

Spectroelectrochemistry

In the course of the electrolysis, the UV-Vis. absorption spectrum of the reacting solution was monitored. It was not possible to see the entire Soret band at this concentration given its high molar extinction coefficient. However, it was observed that the Soret band foot underwent a progressive bathochromic shift, in agreement with the functionalization of the porphyrin by an electrowithdrawing group (Fig. 2).[21] Noteworthy, in CH_2Cl_2 the Soret band of the pure **1-Zn** and **1-Zn-PPh$_3^+$,PF$_6^-$·P(O)Ph$_3$** appears at 414 nm and 432 nm, respectively.

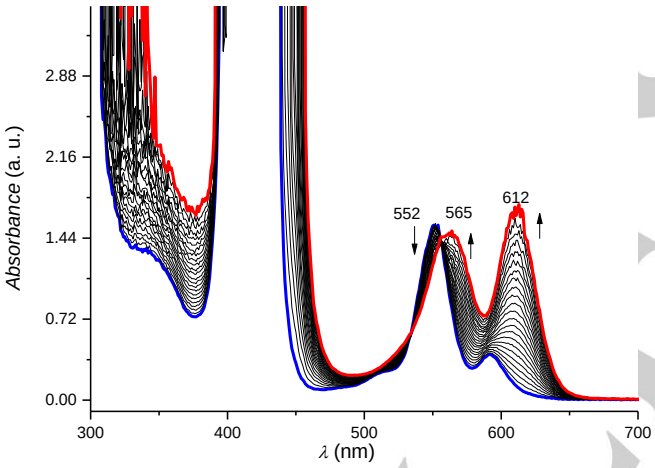

Figure 2. Electrolysis of a 5×10^{-4} M solution of **1-Zn** with 20 eq. PPh_3 and 10 eq. of *2,6*-lutidine followed by UV-Vis. spectroscopy (*l* = 2 mm, 0.1 M $TEAPF_6$ in CH_2Cl_2/CH_3CN (4/1 v/v), E_{app} = 0.70 V *vs*. SCE, -2.4 F, WE: Pt wire, WE and counter-electrode are in separated compartments).

The initial Q band of **1-Zn** (λ_{max} = 552 nm) progressively disappears at the expense of two new bands at 565 and 612 nm. The presence of an isosbestic point located at 557 nm confirms the simple transformation of the initial porphyrin into another well-defined product, **1-Zn-PPh$_3^+$,PF$_6^-$·P(O)Ph$_3$**, with no intermediate observed between.

NMR and Maldi-Tof mass spectrometry characterization of 1-Zn-PPh$_3^+$,PF$_6^-$·P(O)Ph$_3$

From 1D and 2D NMR analyses, the isolated compound was unambiguously identified as the *meso*-substituted triphenylphosphonium porphyrin coordinated at the Zn(II) center by one triphenylphosphonium oxide ($P(O)Ph_3$) molecule (Fig. 3). In particular, the presence of four *β*-pyrrolic doublets between 8.7 and 8.2 ppm (H_d, H_e, H_i and H_j) as well as the disappearance of the singlet signal corresponding to the *meso* proton confirms the functionalization of the porphyrin ring in *meso* position. Moreover, the global integration value (28 H) for the signals located within the common chemical shifts of the phenyl/tolyl groups (7.4-8.0 ppm) is in agreement with the mono-*meso*-substitution.

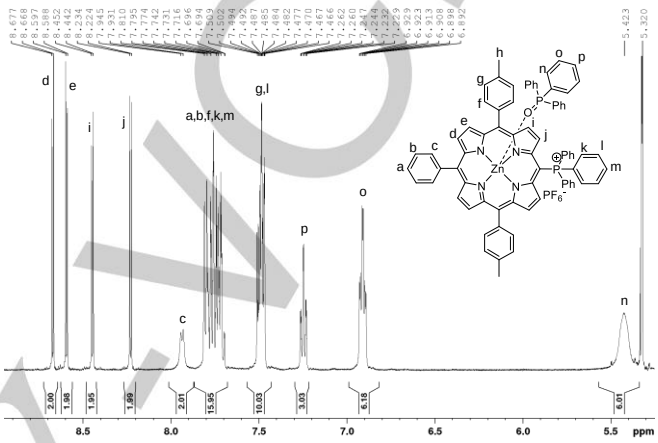

Figure 3. Partial ^{1}H NMR spectra of **1-Zn-PPh$_3^+$,PF$_6^-$·P(O)Ph$_3$** (300 MHz, 298 K, CD_2Cl_2).

As compared to the initial **1-Zn** porphyrin,[17a] an important shielding of the *β*-pyrrolic proton signals H_i (from 9.39 to 8.23 ppm) and H_j (from 9.09 to 8.44 ppm) is observed. This behavior confirms the substitution at the *meso* position by the triphenylphosphonium group since H_i and H_j are under the influence of the shielding cone of the phenyl groups from the phosphonium moiety. Three unexpected signals located between 7.3 and 5.3 ppm are attributed to the aromatic protons from an O-coordinated $P(O)Ph_3$ molecule. As a consequence of the strong influence of the shielding cone of the porphyrin ring, these proton signals (H_n, H_o, H_p) are also highly shielded. In the ^{31}P NMR spectrum, three signals are observed at 26.5, 23.9 and −144.5 ppm for the phosphorus atoms of $P(O)Ph_3$, -PPh_3^+ and PF_6^-, respectively (see ESI).

Analysis of **1-Zn-PPh$_3^+$,PF$_6^-$·P(O)Ph$_3$** by MALDI-TOF mass spectrometry confirms the functionalization of the porphyrin periphery by the phosphonium group. However, the initially coordinated $P(O)Ph_3$ ligand and the PF_6^- anion are not seen on the mass spectrum (see ESI).

X-ray Crystallography

A definite proof of the **1-Zn-PPh$_3^+$,PF$_6^-$·P(O)Ph$_3$** molecular structure was given from the X-ray diffraction analysis. Suitable crystals were obtained by slow diffusion of *n*-hexane into a concentrated CH_2Cl_2 solution of **1-Zn-PPh$_3^+$,PF$_6^-$·P(O)Ph$_3$**. The three-dimensional molecular views of **1-Zn-PPh$_3^+$,PF$_6^-$·P(O)Ph$_3$** are presented in Fig. 4 and Fig. 5. The zinc(II) atom is coordinated by one apical triphenylphosphine oxide molecule (*d*(Zn-O1) = 2.010(4) Å). This Zn-O distance is slightly shorter than the one

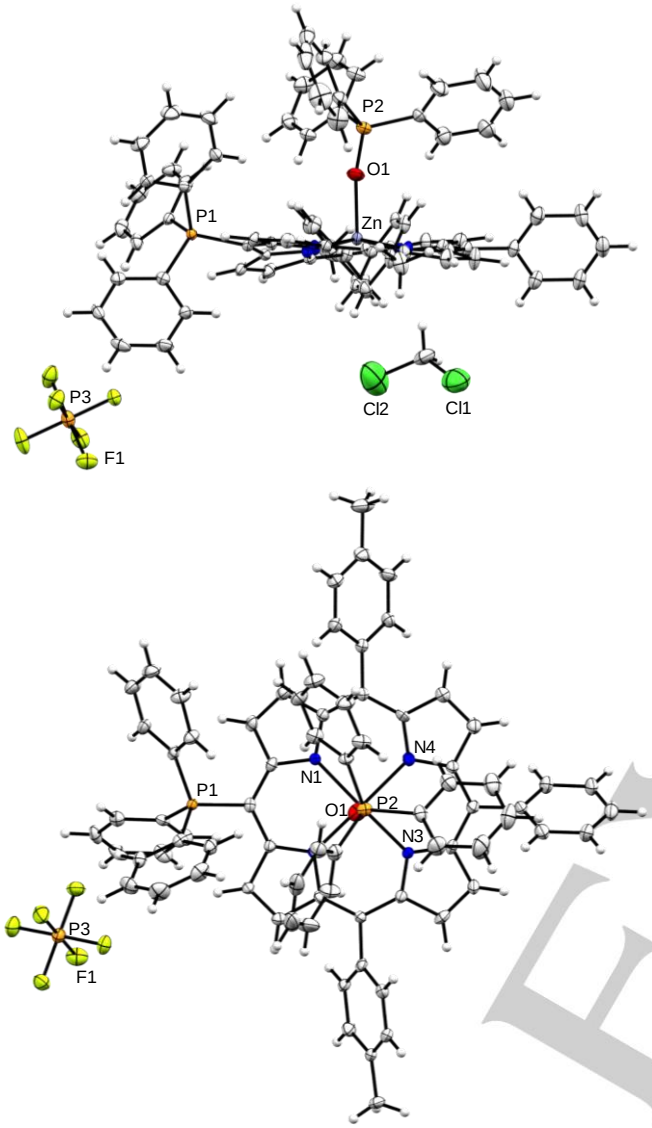

Figure 4. Side (top) and front (bottom) Mercury views of **1-Zn-PPh$_3^+$,PF$_6^-$·P(O)Ph$_3$·CH$_2$Cl$_2$** X-ray crystallographic structure. CH_2Cl_2 molecule was omitted on the front view for clarity. Thermal ellipsoids are scaled to the 50% probability level.

observed for the one-dimensional coordination polymer [10,20-diphenylporphyrinatozinc(II)-5,15-diyl]-bis-[P(O)Ph$_2$]}$_n$·{1.5H$_2$O}$_n$ (*d*(Zn-O) = 2.0224(14) Å) reported by Arnold and coworkers.[4a] The P2-O1 distance (*d*(P2-O1) = 1.490(4) Å) is very close to the one reported in reference [4a] (*d*(P-O) = 1.4899(17) Å) and the Zn-O1-P2 angle (165.5(3)°) is significantly lower than the one found in reference [4a] (177.56(9)°). The presence of one PF$_6^-$ anion per porphyrin molecule confirms the cationic nature of the macrocycle. The CH_2Cl_2 solvent used for the crystallization process is also found in the crystal lattice and it interacts with the porphyrin via C-H···π interaction (*d*(C77-H77B···centroid(N4-C16-C15-C14-C13) = 3.496(11) Å; C77-H77B-centroid(N4-C16-C15-C14-C13) = 171.90(X)°). Each porphyrin interacts with six PF$_6^-$ anions via C···F and H···F interactions (*d*(C64-H64···F1) = 3.170(7) Å; *d*(C63-H63···F4) = 3.304(8) Å; *d*(C62···F1) = 3.127(8) Å; *d*(C62-H62···F2) = 3.207(9) Å; *d*(C61-H61···F5) = 3.398(8) Å; *d*(C74···F4) = 3.091(8) Å; *d*(C23···F5) = 3.169(8) Å; *d*(C24-H24···F3) = 3.257(9) Å; *d*(C34-H34···F6) = 3.231(7) Å; *d*(C29-H29···F2 = 3.138(9) Å; *d*(C30-H30···F3) = 3.301(7) Å; *d*(C30-H30···F4) = 3.511(7) Å).

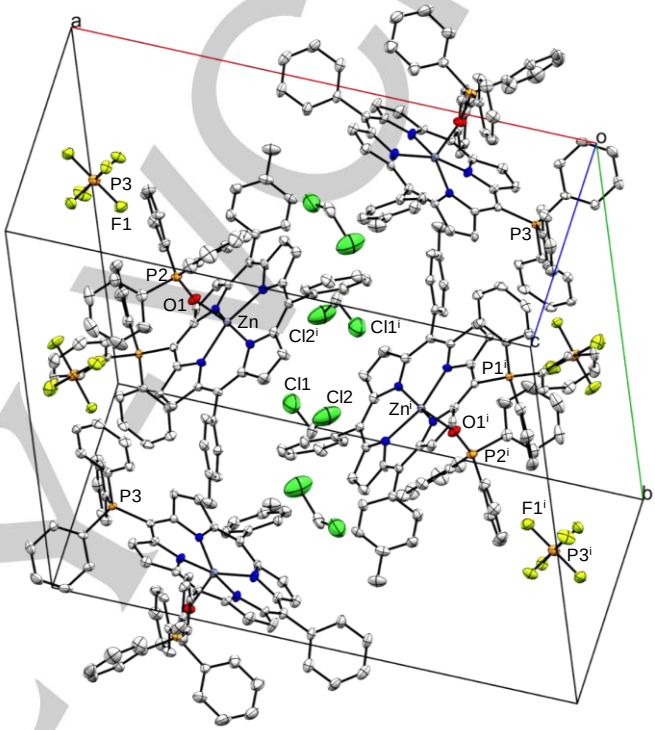

Figure 5. Unit cell of **1-Zn-PPh$_3^+$,PF$_6^-$·P(O)Ph$_3$·CH$_2$Cl$_2$**. H atoms are omitted for clarity. Thermal ellipsoids are scaled to the 50% probability level. [Symmetry code: (i) 1-x, 1-y, 1-z].

Interestingly, these interactions only occur with the phenyl groups from the triphenylphosphine and triphenylphosphine oxide and not with the phenyl/tolyl moieties of the porphyrin ring.

Previously, we synthesized in good yield the *meso*-triphenylphosphonium magnesium(II) porphine **MgP-PPh$_3^+$,PF$_6^-$** by electrochemical oxidation of magnesium(II) porphine (**MgP**) in presence of PPh$_3$, according to Scheme 2.[14]

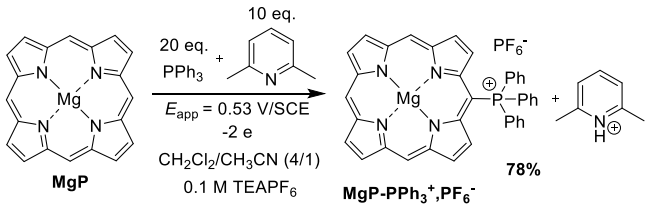

Scheme 2. Electrosynthesis of **MgP-PPh$_3^+$,PF$_6^-$** as reported in reference [14].

Contrary to **1-Zn-PPh$_3^+$,PF$_6^-$·P(O)Ph$_3$**, coordination of P(O)Ph$_3$ molecule was not observed on the ^{1}H and ^{31}P NMR spectra despite the fact that P(O)Ph$_3$ is known to strongly coordinate magnesium(II) porphyrin complexes.[4c] As **MgP-PPh$_3^+$,PF$_6^-$** was generated at lower potential than **1-Zn-PPh$_3^+$,PF$_6^-$·P(O)Ph$_3$** (0.53 V *vs*. 0.70 V), PPh$_3$ is plausibly not oxidized to P(O)Ph$_3$ in these conditions. The X-ray crystallographic structure was solved and toluene and ethanol coming from the crystallization solvents were found in the crystal lattice.[14] Using other crystallization conditions, *i.e.* slow diffusion of diethylether into a concentrated EtOH solution of **MgP-PPh$_3^+$,PF$_6^-$**, suitable crystals of **MgP-PPh$_3^+$,PF$_6^-$·EtOH·H$_2$O·2Et$_2$O** were obtained and this unreported X-ray crystallographic structure is presented in this manuscript for comparison purpose (Fig. 6 and Fig. 7).

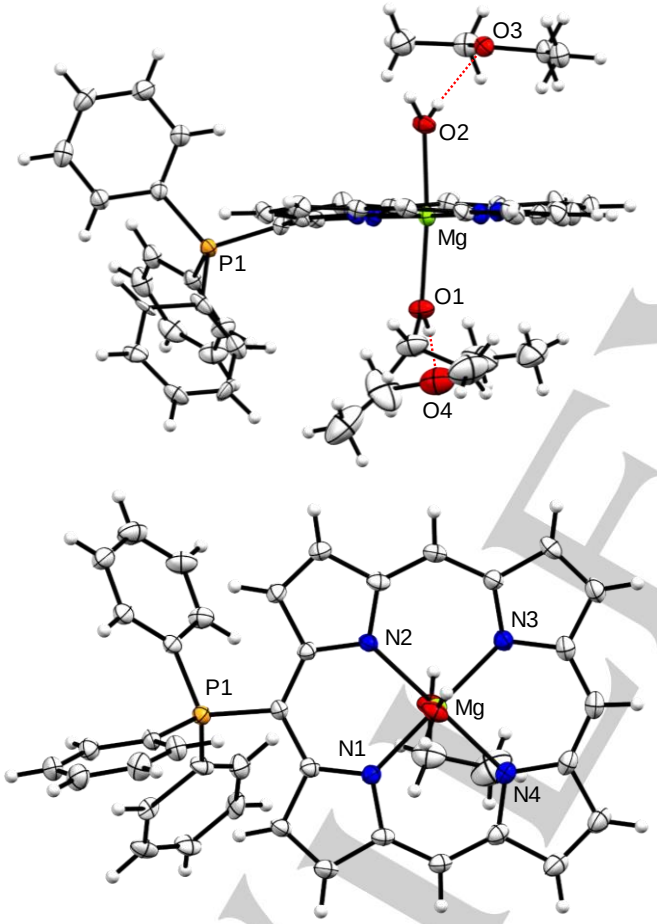

Figure 6. Side (top) and front (bottom) Mercury views of **MgP-PPh$_3^+$,PF$_6^-$·EtOH·H$_2$O·2Et$_2$O** X-ray crystallographic structure. PF$_6^-$ anion is omitted in these views and both Et$_2$O molecules are omitted in the front view for clarity. Thermal ellipsoids are scaled to the 50% probability level.

The magnesium(II) atom is axially coordinated by one H$_2$O (*d*(Mg-O2) = 2.145(3) Å) and one EtOH molecules (*d*(Mg-O1) = 2.190(4) Å). Two porphyrins related by an inversion center form an H-bonded dimer involving two H$_2$O ligands and two Et$_2$O molecules (*d*(O2-H2A···O3) = 2.842(4) Å, *d*(O2-H2B···O3^i) = 2.812(4) Å, O2-H2A-O3 = 176.3(2)°, O2-H2B-O3^i = 176.5(2)°, Fig. 7). The EtOH axial ligand also exhibits an hydrogen bond with an Et$_2$O molecule (*d*(O1-H1···O4) = 2.806(7) Å, O1-H1-O4 = 174(5)°). The presence of one PF$_6^-$ anion per porphyrin molecule confirms the cationic nature of the macrocycle. Each porphyrin interacts with four PF$_6^-$ anions via H···F interactions. As for **1-Zn-PPh$_3^+$,PF$_6^-$·P(O)Ph$_3$**, three interactions between protons from the phenyl rings of the triphenylphosphonium and the fluoride atoms are observed (*d*(C29-H29···F1) = 3.340(5) Å; *d*(C35-H35···F3) = 3.282(5) Å; *d*(C35-H35···F6) = 3.393(5) Å). Besides, two additional H···F interactions exist between *meso*-hydrogen atoms of the porphyrin ring and the hexafluorophosphate anion (*d*(C15-H15···F3) = 3.366(5) Å, *d*(C10-H10···F1) = 3.449(5) Å). Due to the bulkiness of the -PPh$_3$ group, the *meso* C–P$^+$ bond (C20–P1 = 1.785(4) Å) clearly bends towards the exo-position of the dimer and the P atom stands 0.783(2) Å above the 24 atom mean plane of the porphyrin ring.

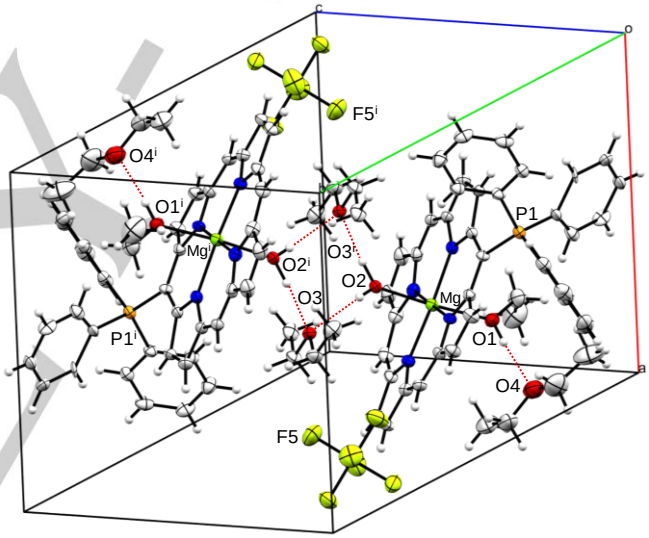

Figure 7. Unit cell of **MgP-PPh$_3^+$,PF$_6^-$·EtOH·H$_2$O·2Et$_2$O**. Thermal ellipsoids are scaled to the 50% probability level. [Symmetry code: (i) 1-x, 1-y, 1-z].

Selected parameters for these novel crystallographic structures are compared with both existing *meso*-triphenylphosphonium Mg(II) and Ni(II) porphyrins[14, 16] and the unique β-substituted triphenylphosphonium Fe(III) porphyrin reported example[9] (Table 1). For these five X-ray crystallographic structures the metal-nitrogen distances are similar for the Zn(II) and Mg(II) complexes (2.063(3) ≤ *d*(M-N) ≤ 2.095(4) Å), slightly lower for the Fe(III) complex (2.042(6) ≤ *d*(M-N) ≤ 2.064(6) Å) and much lower for the Ni(II) complex (1.906(5) < *d*(M-N) < 1.919(5) Å). The C$_{porphyrin}$-P$^+$ bond lengths are all very similar (1.785(4) ≤ *d*(C$_{porphyrin}$-P$^+$) ≤ 1.809(6) Å) and correspond to common bond lengths of aryl-triphenylphosphonium derivatives.[22] The RMS deviation, which is a structural parameter which allows for measuring the distortion magnitude of a macrocycle, was calculated for the Mg(II), Zn(II) and Ni(II) complexes. In the case of porphyrins, the RMS

deviation corresponds to the root mean square of the distances of the 24 carbon and nitrogen porphyrin ring atoms from the mean plane formed by these atoms. The RMS deviation is low for both Mg(II) complexes (0.113 and 0.115 Å for **MgP-PPh$_3^+$,PF$_6^-$·EtOH·H$_2$O·2Et$_2$O** and **MgP-PPh$_3^+$,PF$_6^-$·EtOH·toluene** respectively) while it increases for the Zn(II) porphyrin (0.234 Å) and is much higher for the Ni(II) complex (0.407 Å), highlighting its marked deviation from the planarity.

Table 1. Selected structural parameters for the *meso* and β triphenylphosphonium-porphyrins.

Structural parameters (Å)	**1-Zn-PPh$_3^+$,PF$_6^-$·P(O)PPh$_3$·CH$_2$Cl$_2$**	**MgP-PPh$_3^+$,PF$_6^-$·EtOH·H$_2$O·2Et$_2$O**	**MgP-PPh$_3^+$,PF$_6^-$·EtOH·toluene** [14]	**1-Ni-PPh$_3^+$,PF$_6^-$** [16]	**Fe(III) β-PPh$_3^+$-TPPCl$_2$** [9]
d(M-N)	2.069(4) < d < 2.091(5)	2.063(3) < *d* < 2.081(3)	2.072(3) < *d* < 2.095(4)	1.906(5) < *d* < 1.919(5)	2.042(6) < *d* < 2.064(6)
d(C$_{porphyrin}$-P$^+$)	1.804(5)	1.785(4)	1.794(3)	1.809(6)	1.799(9)
d(P$^+$-mean plane) [a]	0.580	0.783(2)	0.390	1.590	*not reported*
RMS deviation [b]	0.234	0.113	0.115	0.407	*not reported*

[a] mean plane calculated from the 24 carbon and nitrogen porphyrin ring atoms.

[b] The RMS deviation corresponds to the root mean square of the distances of the 24 carbon and nitrogen porphyrin ring atoms from the mean plane formed by these atoms.

Conclusions

In summary the electrochemical oxidation of zinc(II) *5,15-p*-ditolyl-*10*-phenylporphyrin **1-Zn** in the presence of triphenylphosphine (PPh$_3$) affords, in good yield and perfect regioselectivity, *meso*-substituted triphenylphosphonium porphyrin coordinated by one triphenylphosphonium oxide molecule (**1-Zn-PPh$_3^+$,PF$_6^-$·P(O)PPh$_3$**). P(O)Ph$_3$ is thought to come partially from the oxidation of PPh$_3$ during the controlled potential electrolysis. This assertion is strengthened by the fact that the more easily oxidized *meso*-triphenylphosphonium magnesium(II) porphine complex **MgP-PPh$_3^+$,PF$_6^-$** is not coordinated by P(O)Ph$_3$ although Mg(II) porphyrins are known to strongly interact with this ligand. The X-ray crystallographic structures of **Zn-PPh$_3^+$,PF$_6^-$·P(O)PPh$_3$·CH$_2$Cl$_2$** and **MgP-PPh$_3^+$,PF$_6^-$·EtOH·H$_2$O·2Et$_2$O** have been solved and exhibit common structural features of aryl-phosphonium derivatives. This work is part of a more vast research program aiming at improving the control of the oxidative reactivity of metalloporphyrins. Further studies are in progress to improve the scope of the reaction.

Experimental Section

X-ray equipment and refinement

Diffraction data were collected on a Bruker Apex II CCD diffractometer equipped with an Oxford Cryosystems low-temperature device, operating at T = 115 K. Data were measured using ϕ and ω scans using MoK$_\alpha$ radiation (X-ray tube, 50 kV, 32 mA). The total number of runs and images was based on the strategy calculation from the program APEX2.[23] Cell parameters were retrieved using the SAINT[23] software and refined using SAINT. Data reduction was performed using the SAINT software which corrects for Lorentz polarisation. A multi-scan absorption correction was performed using SADABS[23] was used for absorption correction. Using Olex2,[24] the structure was solved with the ShelXS[25] structure solution program, using the direct phasing methods solution method. The model was refined with version 2018/3 of ShelXL[26] using Least Squares minimisation.

A single violet prism-shaped crystal (0.15×0.15×0.10) mm^3 of (**1-Zn-PPh$_3^+$,PF$_6^-$·P(O)Ph$_3$·CH$_2$Cl$_2$**) was mounted on a mylar loop with oil. The structure was solved in the space group P2$_1$/c (# 14). All non-hydrogen atoms were refined anisotropically. Hydrogen atom positions were calculated geometrically and refined using the riding model. One solvent dichloromethane molecule was identified but is disordered over several positions. Only one component of the disorder was unambiguously localized with an occupation factor converged to 0.45. The data were corrected for the residual electron density due to the other components of the solvate molecule by the Squeeze procedure.[27]

A single violet prism-shaped crystals (0.15×0.08×0.03) mm^3 of (**MgP-PPh$_3^+$,PF$_6^-$·EtOH·H$_2$O·2Et$_2$O**) was mounted on a mylar loop with oil. The structure was solved in the space group P-1 (# 2). Most hydrogen atom positions were calculated geometrically and refined using the riding model, but hydrogen atoms bonded to oxygen atoms were refined using geometric restraints. One of the phenyl group was found disordered over two positions with occupation factors converged to 0.59:0.41, the minor component was isotropically refined. One ethanol and one water molecules are linked to the Mg atom in axial position. The ethanol molecule was found slightly disordered over two positions with occupation factors converged to 0.81:0.19, the minor component was isotropically refined. SADI restraints were applied on the two ether molecules.

CCDC-1848217 (**1-Zn-PPh$_3^+$,PF$_6^-$·P(O)Ph$_3$·CH$_2$Cl$_2$**) and CCDC-1848218 (**MgP-PPh$_3^+$,PF$_6^-$·EtOH·H$_2$O·2Et$_2$O**) contains the supplementary crystallographic data for this paper. These data can be obtained free of charge from The Cambridge Crystallographic Data Centre via www.ccdc.cam.ac.uk/data_request/cif.

Reagents and instrumentation

Porphyrin **1-Zn** was synthesized according to known procedures.[28] Our data (^{1}H NMR, ^{13}C NMR, UV-Vis. absorption, and MALDI-TOF mass spectrum) were consistent with those described in reference [28] (see ESI). Tetraethylammonium hexafluorophosphate (TEAPF$_6$, Fluka puriss., electrochemical grade, ≥ 99.0%) and *2,6*-lutidine (Aldrich, purified by redistillation, ≥ 99%) were used as received. CH$_2$Cl$_2$ (Carlo Erba 99.5%)

and CH_3CN (SDS, Carlo Erba, HPLC gradient 99.9%) were distilled from P_2O_5 and CaH_2 respectively.

UV-Vis. absorption spectra were obtained with a Varian UV-vis spectrophotometer Cary 50 scan using quartz cells (Hellma). In spectroelectrochemical experiments, an UV-Vis. immersion probe (Hellma, *l* = 2 mm) was connected through optical fibers to the same spectrophotometer.

Mass spectra were obtained on a Bruker ProFLEX III spectrometer (MALDI-TOF) using dithranol as a matrix.

NMR spectra were measured on a BRUKER 300, 500 or 600 MHz spectrometer (Avance III Nanobay, Avance III, Avance II, respectively). The reference was the residual non-deuterated solvent.

All electrochemical manipulations were performed using Schlenk techniques in an atmosphere of dry oxygen-free argon at room temperature (T = 20°C ± 3°C). The supporting electrolyte was degassed under vacuum before use and then dissolved to a concentration of 0.1 mol L^{-1}. Voltammetric analyses were carried out in a standard three-electrode cell, with an Autolab PGSTAT 302 N potentiostat, connected to an interfaced computer that employed Electrochemistry Nova software. The reference electrode was a saturated calomel electrode (SCE) separated from the analyzed solution by a sintered glass disk filled with the background solution. The auxiliary electrode was a platinum wire separated from the analyzed solution by a sintered glass disk filled with the background solution. For all voltammetric measurements, the working electrode was a platinum disk electrode (Ø = 2 mm). In these conditions, when operating in a mixture of CH_2Cl_2/CH_3CN 4/1 (0.1 M $TEAPF_6$) the formal potential for the Fc^+/Fc couple was found to be +0.40 V *vs.* SCE.

Bulk electrolyses were performed in a two or three compartment cell with glass frits of medium porosity with an Amel 552 potentiostat coupled with an Amel 721 electronic integrator. A platinum wire spiral (*l* = 53 cm, Ø = 1 mm) was used as the working electrode, a platinum plate as the counter electrode and a saturated calomel electrode as the reference electrode. Electrolyses were followed by TLC and UV-Vis. absorption measurements.

Electrosynthesis of 1-Zn-PPh_3^+,PF_6^-·P(O)Ph_3

Electrolyses were carried out under argon, at room temperature, in 40 mL of CH_2Cl_2/CH_3CN (4/1 v/v) containing 0.1 M of $TEAPF_6$, 20.0 mg (31.74 µmol) of **1-Zn**, 10 eq. of *2,6*-lutidine (37 µl) and 20 eq. of PPh_3 (166.5 mg). The applied potential was E_{app} = 0.70 V *vs.* SCE. At the end of the electrolysis, 2.4 F per mol of **1-Zn** were transferred. The solution mixture was then evaporated to dryness under reduced pressure. The resulting crude solid was dissolved in a minimum of CH_2Cl_2 and this solution was washed with 3×250 mL of distilled water to remove the supporting electrolyte. The organic phase was evaporated to dryness. The crude product was then purified using silica gel column chromatography (CH_2Cl_2), recrystallized from toluene providing **1-Zn-PPh_3^+,PF_6^-·P(O)Ph_3** in 84% yield (*m* = 35.0 mg). ^{1}H NMR (CD_2Cl_2, 500 MHz, 298 K) : δ (ppm) 2.64 (s, CH_3, 6H), 5.42 (s, *o*-Ph, 6H), 6.88-6.95 (m, *m*-Ph, 6H), 7.46-7.52 (m, *p*-Ph, 3H), 7.46-7.52 (m, *m*-tol, *m*-Ph, 10H) 7.68-7.82 (m, *p- and m*-Ph, *o*-tol, 16H), 7.93-7.95 (m, *o*-Ph, 2H), 8.23 (d, ^3J = 4.9 Hz, *β*-Pyrr, 2H), 8.45 (d, ^3J = 4.9 Hz, *β*-Pyrr, 2H), 8.59 (d, ^3J = 4.6 Hz, *β*-Pyrr, 2H), 8.67 (d, ^3J = 4.6 Hz, *β*-Pyrr, 2H) ; ^{31}P (CD_2Cl_2, 202 MHz, 298 K): δ (ppm) -144.5 (m, PF_6^-), 23.9 (s, P^+), 26.5 (s, P=O) ; RMN ^{13}C (CD_2Cl_2, 125 MHz, 298 K): 126.6, 126.9, 127.3, 127.6, 128.2, 128.4, 128.5, 128.9, 129.1, 129.6, 129.6, 129.7, 130.4, 130.5, 130.6, 132.2, 133.7, 133.9, 134.4, 134. 6, 134.7, 134.8, 138.1, 139.4, 142.3, 148.8, 150.2, 152.8, 153.6. λ_{max} (CH_2Cl_2)/nm (log ε) 432 (5.52), 567 (4.11), 608 (4.29). Maldi-Tof MS (dithranol): cald for $C_{58}H_{42}N_4PZn$ [M $-PF_6^-$ $-P(O)Ph_3]^+$ = 889.24 found 888.91.

Acknowledgements

This work was supported by the CNRS, Université de Bourgogne Franche-Comté, Conseil Régional de Bourgogne through the Plan d'Actions Régional pour l'Innovation (PARI) and the Fonds Européen de Développement Régional (FEDER) programs. A.K.D.D. acknowledges the Ministère de l'Enseignement Supérieur et de la Recherche for a PhD grant and the Université Alioune Diop de Bambey for funding. C.H.D. thanks the CNRS (Sept. 2015, one year ''délégation CNRS'') and the Agence Nationale de la Recherche for funding (ANR-15-CE29-0018-01). The authors are thankful to Dr B. Habermeyer (PorphyChem Company) for generous gift of the 5,15-ditolyporphyrin sample and to S. Fournier for technical support.

Keywords: Phosphorus • Porphyrinoids • Molecular electrochemistry • Electrosynthesis • Radical reactions

[1] I. Beletskaya, V. S. Tyurin, A. Y. Tsivadze, R. Guilard, C. Stern, *Chem. Rev.* **2009**, *109*, 1659-1713.

[2] a) F. J. Kampas, K. Yamashita, J. Fajer, *Nature* **1980**, *284*, 40-42; b) E. Song, C. Shi, F. C. Anson, *Langmuir* **1998**, *14*, 4315-4321; c) C. Bucher, C. H. Devillers, J.-C. Moutet, G. Royal, E. Saint-Aman, *Chem. Commun.* **2003**, 888-889; d) H. Imahori, M. Kimura, K. Hosomizu, T. Sato, T. K. Ahn, S. K. Kim, D. Kim, Y. Nishimura, I. Yamazaki, Y. Araki, O. Ito, S. Fukuzumi, *Chem. Eur. J.* **2004**, *10*, 5111-5122; e) L. Wei, K. Padmaja, W. J. Youngblood, A. B. Lysenko, J. S. Lindsey, D. F. Bocian, *J. Org. Chem.* **2004**, *69*, 1461-1469; f) M. R. Wasielewski, *Acc. Chem. Res.* **2009**, *42*, 1910-1921.

[3] Y. Matano, in *Main Group Strategies for Functional Hybrid Materials* (Eds.: T. Baumgartner, F. Jäckle), Wiley, **2018**, pp. 265-293.

[4] a) F. Atefi, J. C. McMurtrie, P. Turner, M. Duriska, D. P. Arnold, *Inorg. Chem.* **2006**, *45*, 6479-6489; b) F. Atefi, O. B. Locos, M. O. Senge, D. P. Arnold, *J. Porphyrins Phthalocyanines* **2006**, *10*, 176-185; c) F. Atefi, J. C. McMurtrie, D. P. Arnold, *Dalton Trans.* **2007**, 2163-2170; d) Y. Matano, K. Matsumoto, Y. Nakao, H. Uno, S. Sakaki, H. Imahori, *J. Am. Chem. Soc.* **2008**, *130*, 4588-4589; e) Y. Y. Enakieva, A. G. Bessmertnykh, Y. G. Gorbunova, C. Stern, Y. Rousselin, A. Y. Tsivadze, R. Guilard, *Org. Lett.* **2009**, *11*, 3842-3845; f) K. M. Kadish, P. Chen, Y. Y. Enakieva, S. E. Nefedov, Y. G. Gorbunova, A. Y. Tsivadze, A. Bessmertnykh-Lemeune, C. Stern, R. Guilard, *J. Electroanal. Chem.* **2011**, *656*, 61-71; g) Y. Matano, K. Matsumoto, T. Shibano, H. Imahori, *J. Porphyrins Phthalocyanines* **2011**, *15*, 1172-1182; h) E. V. Vinogradova, Y. Y. Enakieva, S. E. Nefedov, K. P. Birin, A. Y. Tsivadze, Y. G. Gorbunova, A. G. Bessmertnykh Lemeune, C. Stern, R. Guilard, *Chem. - Eur. J.* **2012**, *18*, 15092-15104; i) Y. Matano, K. Matsumoto, H. Hayashi, Y. Nakao, T. Kumpulainen, V. Chukharev, N. V. Tkachenko, H. Lemmetyinen, S. Shimizu, N. Kobayashi, D. Sakamaki, A. Ito, K. Tanaka, H. Imahori, *J. Am. Chem. Soc.* **2012**, *134*, 1825-1839; j) K. Fujimoto, Y. Kasuga, N. Fukui, A. Osuka, *Chem. - Eur. J.* **2017**, *23*, 6741-6745; k) K. Fujimoto, H. Yorimitsu, A. Osuka, *Org. Lett.* **2014**, *16*, 972-975; l) N. Fukui, S.-K. Lee, K. Kato, D. Shimizu, T. Tanaka, S. Lee, H. Yorimitsu, D. Kim, A. Osuka, *Chem. Sci.* **2016**, *7*, 4059-4066.

[5] Y. Matano, K. Matsumoto, Y. Terasaka, H. Hotta, Y. Araki, O. Ito, M. Shiro, T. Sasamori, N. Tokitoh, H. Imahori, *Chem. - Eur. J.* **2007**, *13*, 891-901.

[6] K. L. Bergeron, E. L. Murphy, O. Majofodun, L. D. Muñoz, J. C. Williams, K. H. Almeida, *Mutat. Res.* **2009**, *673*, 141-148.

[7] a) B. Evans, K. M. Smith, *Tetrahedron Lett.* **1977**, *18*, 3079-3082; b) K. M. Smith, G. H. Barnett, B. Evans, Z. Martynenko, *J. Am. Chem. Soc.* **1979**, *101*, 5953-5961.

[8] a) A. G. Padilla, S.-M. Wu, H. J. Shine, *J. Chem. Soc., Chem. Commun.* **1976**, 236-237; b) H. J. Shine, A. G. Padilla, S.-M. Wu, *J. Org. Chem.* **1979**, *44*, 4069-4075.

[9] A. Malek, L. Latos-Grazynski, T. J. Bartczak, A. Zadlo, *Inorg. Chem.* **1991**, *30*, 3222-3230.

[10] A. Giraudeau, L. El Kahef, *Can. J. Chem.* **1991**, *69*, 1161-1165.

[11] L. Ruhlmann, A. Giraudeau, *Chem. Commun.* **1996**, 2007-2008.

[12] a) L. Ruhlmann, A. Giraudeau, *Eur. J. Inorg. Chem.* **2001**, 659-668; b) L. Ruhlmann, M. Gross, A. Giraudeau, *Chem. - Eur. J.* **2003**, *9*, 5085-5096.

[13] a) C. H. Devillers, D. Lucas, A. K. D. Dimé, Y. Rousselin, Y. Mugnier, *Dalton Trans.* **2010**, *39*, 2404-2411; b) C. H. Devillers, A. K. D. Dimé, H. Cattey, D. Lucas, *C. R. Chim.* **2013**, *16*, 540-549; c) C. H. Devillers, P. Fleurat-Lessard, D. Lucas, in *Handbook of Porphyrin Science, Vol. 37* (Eds.: K. M. Kadish, K. M. Smith, R. Guilard), World Scientific Publishing Company, **2016**, pp. 75-231.

[14] C. H. Devillers, A. K. D. Dimé, H. Cattey, D. Lucas, *Chem. Commun.* **2011**, *47*, 1893-1895.

[15] M. A. Vorotyntsev, D. V. Konev, C. H. Devillers, I. Bezverkhyy, O. Heintz, *Electrochim. Acta* **2010**, *55*, 6703.

[16] A. K. D. Dimé, C. H. Devillers, H. Cattey, D. Lucas, *Dalton Trans.* **2014**, *43*, 14554-14564.

[17] a) A. K. D. Dimé, C. H. Devillers, H. Cattey, B. Habermeyer, D. Lucas, *Dalton Trans.* **2012**, *41*, 929-936; b) K. M. Kadish, E. V. Caemelbecke, G. Royal, in *The Porphyrin Handbook, Vol. 8* (Eds.: K. M. Kadish, K. M. Smith, R. Guilard), Academic Press, **2000**, pp. 1-114.

[18] A. Giraudeau, L. Ruhlmann, L. El Kahef, M. Gross, *J. Am. Chem. Soc.* **1996**, *118*, 2969-2979.

[19] J. H. Fuhrhop, K. M. Kadish, D. G. Davis, *J. Am. Chem. Soc.* **1973**, *95*, 5140-5147.

[20] Y. M. Kargin, Y. G. Budnikova, *Russ. J. Gen. Chem.* **2001**, *71*, 1393-1421.

[21] K. M. Kadish, R. K. Rhodes, *Inorg. Chem.* **1981**, *20*, 2961-2966.

[22] a) L. E. Longobardi, P. Zatsepin, R. Korol, L. Liu, S. Grimme, D. W. Stephan, *J. Am. Chem. Soc.* **2017**, *139*, 426-435; b) S. Nieto, P. Metola, V. M. Lynch, E. V. Anslyn, *Organometallics* **2008**, *27*, 3608-3610; c) H. Kawai, W. J. Wolf, A. G. DiPasquale, M. S. Winston, F. D. Toste, *J. Am. Chem. Soc.* **2016**, *138*, 587-593.

[23] Bruker, Bruker AXS Inc., Madison, Wisconsin, USA, **2014**.

[24] O. V. Dolomanov, L. J. Bourhis, R. J. Gildea, J. A. K. Howard, H. Puschmann, *J. Appl. Cryst.* **2009**, *42*, 339-341.

[25] G. M. Sheldrick, *Acta Cryst. A* **2008**, *64*, 112-122.

[26] G. M. Sheldrick, *Acta Cryst.* **2015**, *C71*, 3-8.

[27] A. Spek, *J. Appl. Cryst.* **2003**, *36*, 7-13.

[28] B. Habermeyer, A. Takai, C. P. Gros, M. E. Ojaimi, J.-M. Barbe, S. Fukuzumi, *Chem. - Eur. J.* **2011**, *17*, 10670-10681.

WILEY-VCH

Entry for the Table of Contents (Please choose one layout)

Layout 1:

FULL PAPER

A Zn(II) *meso*-triaryltriphenylphosphonium porphyrin was electrosynthesized in good yield *via* the electrochemical oxidation of Zn(II) *meso*-triarylporphyrin in the presence of triphenylphosphine. Its X-ray crystallographic structure was solved and was compared with the original Mg(II) *meso*-phosphonium porphine and the already published *meso*- and β-triphenylphosphonium porphyrins.

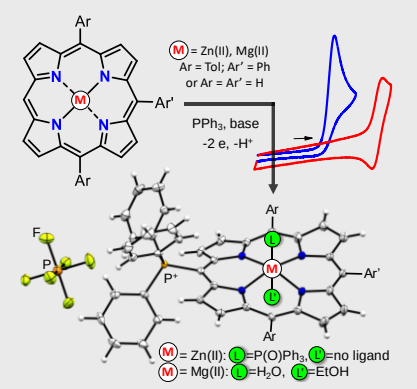

Phosphorus-Based Porphyrins

*Abdou K. D. Dimé, Hélène Cattey, Dominique Lucas and Charles H. Devillers**

Page No. – Page No.

Electrosynthesis and X-ray crystallographic structure of Zn(II) *meso*-triaryltriphenylphosphonium porphyrin and structural comparison with Mg(II) *meso*-triphenylphosphonium porphine

Layout 2:

FULL PAPER

((Insert TOC Graphic here; max. width: 11.5 cm; max. height: 2.5 cm; NOTE: the final letter height should not be less than 2 mm.))

Text for Table of Contents

Key Topic*

*Author(s), Corresponding Author(s)**

Page No. – Page No.

Title

*one or two words that highlight the emphasis of the paper or the field of the study

WILEY-VCH